Aalto University

Wiberg, Cedrik; Busch, Michael; Evenäs, Lars; Ahlberg, Elisabet

The electrochemical response of core-functionalized naphthalene Diimides (NDI) – a combined computational and experimental investigation

Note

The electrochemical response of core-functionalized naphthalene Diimides (NDI) – a combined computational and experimental investigation

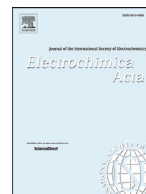Cedrik Wiberg[b], Michael Busch[c,*], Lars Evenäs[b], Elisabet Ahlberg[a,*]

[a] *Department of Chemistry and Molecular Biology, Gothenburg University, 412 96 Gothenburg, Sweden*
[b] *Department of Chemistry and Chemical Engineering, Chalmers University of Technology, 412 96 Gothenburg, Sweden*
[c] *Department of Chemistry and Materials Science, Aalto University, 000 76 Aalto, Finland*

ABSTRACT

Aqueous organic redox flow batteries (AORFBs) have attracted increased interest as sustainable energy storage devices due to the desire of increasing electricity production from renewable energy sources. Several organic systems have been tested as redox active systems in AORFBs but few fundamental electrochemical studies exist. This article provides reduction potentials and acid constants, pK_a, of nine different core-substituted naphthalene diimides (NDI), calculated using density functional theory (DFT). Reduction potentials were acquired at each oxidation state for the nine species and were used to achieve a correlation between the electron donating ability of the substituents and the potential. Cyclic voltammograms were simulated using the scheme-of-squares framework to include both electron and proton transfer processes. The results show that the anion radical is unprotonated in the entire pH range, while the dianion can be protonated in one or two steps depending on the substituent. The core substituents may also have acid-base properties. and optimization of the redox properties for battery applications can therefore be obtained both by changing the core substituent and by changing pH of the electrolyte.

Three core-substituted NDI molecules were studied experimentally and good qualitative agreement with the theoretically predicted behaviour was demonstrated. For 2,6-di(dimethylamino)-naphthalene diimide (2DMA-NDI), the calculations showed that one of the DMA substituents could be protonated in the accessible pH range and pK_a was determined to 3.95 using ^{1}H NMR spectroscopy.

The redox mechanism of each molecule was explored and the qualitative agreement between theory and experiment clearly shows that this combination provides a better understanding of the systems and offers opportunities for further developments. The applicability of NDI for redox flow batteries is finally discussed.

1. Introduction

In the pursuit of environmentally friendly energy storage solutions for large-scale applications, an increasing amount of attention is being directed to the development of aqueous organic redox flow batteries (AORFBs) [1–5]. Employing organic molecules as the redox-active material has the potential of yielding significant advantages in terms of cost and environmental benignity over current technologies which typically rely on lithium, cobalt and vanadium [6].

The most common type of organic substances used in AORFBs is based on quinones, due to their ubiquity, chemical stability and electrochemical reversibility [7]. Many AORFB systems with impressive performance have been reported [6,8,9], but self-association [10,11] and chemical stability [7,12] are areas that hold potential for improvement. While many groups have worked on testing flow batteries with different combinations of organic molecules and reporting their performance [1–5], little research focus has been directed on studying the fundamental chemistry and electrochemistry of organic molecules in the context of their applicability in AORFBs.

* Corresponding authors.
E-mail addresses: michael.busch@aalto.fi (M. Busch), lars.evenas@chalmers.se (L. Evenäs), elisabet.ahlberg@gu.se, ela@chem.gu.se (E. Ahlberg).

One type of molecule that has recently been considered for use in AORFBs is naphthalene diimide (NDI) [13]. NDI is a quinone-like molecule with two imide groups attached to a naphthalene core. The self-associative properties as well as its solubility can be modified by choice of the side chain, which reaches from the imide nitrogen. On the other hand, the electronic properties of NDI can be tuned by chemical substitution on the naphthalene core, giving a large flexibility in the design of the molecule [14]. With the chemical similarity between NDI and quinones, a deeper investigation of NDIs for use in redox flow batteries is merited [15]. NDI has been widely used as acceptor and interlayer in organic solar cells [16], in organic field effect transistors [16], as DNA intercalator [17,18] as well as for sensor applications [19,20]. Electrochemically, NDI has mainly been explored in organic solvents and solid-state batteries [15,21–26] but less in aqueous systems [13], although it has recently been tested in a redox flow battery setup [27]. Furthermore, an NDI-based polymer was used as a solid-state redox-booster for 9,10-anthraquinone-2,7-disulfonic acid (AQDS), increasing the capacity of the negative electrolyte beyond that of unboosted AQDS [28].

Previously, our group evaluated the electrochemical properties of an N-propyl-dimethylamino naphthalene diimide. The molecule, which in the present article is called 2H-NDI, demonstrated a high chemical stability and two reversible redox couples at suitable potentials for AORFB applications [13].

In order to better understand and optimize the properties of NDI for different applications, it is important to study the relationship between the chemical structures of the molecules, and their reduction potential and pH dependencies. The electrochemical behavior of quinones and quinone-like compounds can be described by a system called the *scheme of squares*, in which an n-electron reduction of a quinone can be coupled to between 0 and n protons, opening up $(n + 1)^2$ possible species depending on the applied potential and pH of the solution [18,29,30]. For a complete characterization of the electrochemistry using the scheme of squares of a nine-component system, at least six reduction potentials and six pK_a values are required. Many, if not most, of these are not possible to acquire experimentally, and a computational treatment is therefore helpful.

In the present article, the electrochemical behavior of NDI with different substituents on the naphthalene core was investigated. Reduction potentials and pK_a values at each state of oxidation and protonation of nine different core-substituted NDI molecules were acquired using density functional theory (DFT). These values were used to simulate cyclic voltammograms (CV). Three out of the nine species were synthesized and characterized electrochemically. The investigated NDI molecules are referred to in the text as 2X-NDI, where X denotes a substituent on the naphthalene core. The chemical structures of 2X-NDI are shown in Fig. 1.

2. Experimental

All electrochemical measurements were done in triplicate. **Cyclic Voltammetry:** Prior to each experiment, a glassy carbon working electrode (3 mm in diameter, BASI) was polished with 0.3 μm alumina (Struers AP-D Suspension) and sonicated in deionized water for about one minute. A platinum mesh counter electrode was used together with a reference electrode with Ag/AgCl in 3 M NaCl (BASI) that has a potential of 0.214 V vs she. Cyclic voltammograms at pH 0 and 1 were collected using 1 M and 0.1 M solutions of H_2SO_4 while the remaining solutions were prepared by dissolving 1 mM of material in a pH 7 stock solution of Britton-Robinson Universal buffer. The pH was adjusted with either 1 mM analyte NDI in 0.5 M HCl or neat 1 M NaOH [35]. Voltammograms at scan rates of 20, 50 and 100, 250 and 500 mV/s were collected with a 90% iR-correction by positive feedback. The CVs
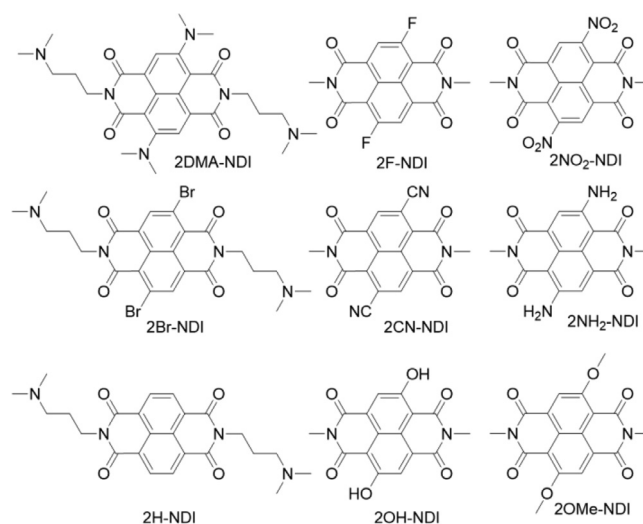
Fig. 1. Chemical structures of the investigated 2X-NDI molecules. For the DFT calculations, CH_3-truncated structures were used for all molecules. The three leftmost structures were investigated experimentally.

were collected in random order with regards to scan rate. **NMR spectroscopy:** A Varian 400 MHz spectrometer was used to record all spectra. The probe was a Varian OneNMRProbe with a proton observe frequency of 399.95 MHz. **pH measurements** were performed using a Metrohm 827 pH lab pH-meter calibrated using buffer solutions (VWR) with pH = 9.00, 7.00 and 4.00. **pK_a measurements:** For 2DMA-NDI, the pK_a was measured using ^{1}H NMR spectroscopy. A stock solution containing 2 mM of imidazole, formic acid, and 2-amino-2-(hydroxymethyl)propane-1,3-diol (tris) as pH indicators, 0.2 mM 3-(trimethylsilyl)propionic-2,2,3,3-d4 acid sodium salt (TSP-D4) as NMR reference as well as 0.5 mM 2DMA-NDI in 90% H_2O/10% D_2O was prepared. In one aliquot, the pH was adjusted by addition of concentrated HCl to approximately pH = 1, and in another, the pH was raised to about 12 by addition of solid NaOH. In order to keep a constant ionic strength throughout the series, 0.09 M NaCl was added to the alkaline sample. An NMR spectrum with water suppression was collected immediately after preparation of the highest pH samples, as 2DMA-NDI hydrolyzed after about an hour, seen by the strongly blue solution turning first green, then yellow. Intermediate pH values were acquired by combining the acidic and the alkaline aliquots in differing proportions. The experiment was repeated with 2 mM piperazine instead of imidazole, formic acid and tris, in order to account for associative effects between the analyte and the pH reference molecules. Reported values for pH-shift relationships for the pH reference molecules were used to determine solution pH based on the measured shift [31]. Calculations and titration curves are given in Section 8 in the SI.

2.1. Synthesis

2.1.1. 2H-NDI

(2,7-bis(3-(dimethylamino)propyl)benzo[lmn][3,8]phenanthroline-1,3,6,8(2H,7H)-tetraone)

2H-NDI was synthesized according to previously described procedures [13,32].

2.1.2. 2Br-NDI (4,9-dibromo-2,7-bis(3-(dimethylamino)propyl)benzo[lmn][3,8]phenanthroline-1,3,6,8(2H,7H)-tetraone)

A slightly modified procedure to the one given in the literature [33] was used for the bromination of NDI: 17.06 g of NDI (39.1 mmol) was dissolved in 37 ml of sulfuric acid in a 100 ml

flask resulting in a dark solution. After all the NDI had been dissolved, 6.76 g (23.6 mmol, 0.61 eq) of dibromantin (1,3-dibromo-5,5-dimethylhydantoin) was added and the flask was stoppered with a rubber septum and left stirring at room temperature. After 18 h, an additional 3.39 g (11.9 mmol, 0.3 eq) of dibromantin was added and the reaction was left for another 20 h. 1.03 g (3.6 mmol, 0.09 eq) of dibromantin was added as the final portion and the reaction left for 22 h. The thick orange mixture was quenched by pouring it into icy water. KOH pellets were added under stirring at 0 °C until the solution turned a gray orange hue. The suspension was extracted three times with chloroform, which was in turn evaporated, washed with hexane and acetone (it was found that acetone partially washes away the monobrominated species) and finally recrystallized from chloroform yielding 12 g of a very fine orange powder. Yield: 52%.

^{1}H NMR (400 MHz, Chloroform-d) δ 8.98 (s, 2H), 4.31 – 4.22 (m, 4H), 2.45 (t, $J = 7.0$ Hz, 4H), 2.24 (s, 12H), 1.99 – 1.85 (m, 4H). ^{13}C NMR (101 MHz, Chloroform-d) δ 160.79, 160.75, 138.99, 128.28, 127.70, 125.32, 124.10, 57.06, 45.23, 39.90, 25.54.

2.1.3. 2DMA-NDI (4,9-bis(dimethylamino)−2,7-bis(3-(dimethylamino)propyl)benzo[lmn][3,8]phenanthroline-1,3,6,8(2H,7H)-tetraone)

5 g (8.4 mmol) of 2Br-NDI was added to a 100 ml double-necked round-bottom flask and purged three times by alternating between vacuum and nitrogen. 15 ml of 2 M (30 mmol, 3.57 eq) dimethylamine in THF was added and the blood-red mixture was left stirring under reflux. After 18 h, the mixture was evaporated into a thick black oil which was dissolved in chloroform and washed with alkaline water in a separating funnel. The organic phase was dried, and the remaining material was recrystallized from isopropanol to yield 3.62 g of a dark blue powder. Yield: 82%.

^{1}H NMR (400 MHz, Deuterium Oxide) δ 7.94 (s, 2H), 4.09 (t, $J = 6.9$ Hz, 4H), 3.30 – 3.23 (m, 4H), 3.01 (s, 12H), 2.91 (s, 12H), 2.16 – 2.07 (m, 4H). ^{13}C NMR (101 MHz, Deuterium Oxide) δ 163.98, 161.38, 151.25, 123.36, 122.53, 122.24, 105.22, 55.32, 43.31, 42.69, 37.39, 22.99.

2.2. Computational details

All molecules shown in Fig. 1 were studied using density functional theory (DFT). In the calculations, the dimethylamino-propyl groups attached to the imide nitrogens were replaced by CH_3-groups to reduce the computational costs. Owing to the fact that these groups are not directly involved in the chemistry at the NDI core, this simplification is expected to not affect the predictive power of the calculations adversely.

The DFT calculations were performed using Gaussian 16 Rev. B.01 [34] in combination with the M06–2X functional and a triple-z 6–311++G^{**} basis set with diffuse and polarization functions on all atoms [35]. The M06–2X functional was chosen based on its well-proven performance for organic molecules [36] and electron transfer potentials of small organic molecules [34]. Solvation was treated using the implicit SMD solvation model as implemented into Gaussian 16 [38]. Convergence of the structures to the minimum was ensured by testing for, and removal of, all imaginary frequencies.

Proton-coupled electron transfer reactions (PCET) were modeled using the computational standard hydrogen electrode [39] which assumes the formation of H_2 upon proton abstraction. For example, for the oxidation of an arbitrary compound A-H to A Reaction 1 is assumed:

$$A - H \rightarrow A + 0.5H_2 \tag{1}$$

This offsets the computation with the she scale and changes to the redox potential due to pH effects can be estimated using the Nernst equation. Electron transfer (ET) potentials were computed using the effective absolute potential method [34] to pre-compute an effective absolute potential (E_{abs}(eff; she)) for the given computational setup from a reference acid-base reaction. Formic acid dissociation (pK_a=3.77) was used as reference system [35]. E_{abs}(eff; she) can be used to offset the absolute reduction or oxidation potential to the she scale. Accordingly, the reduction potential of the ET reactions (E_{red}(ET; she)) was computed as follows:

$$E_{red}(ET; she) = E(reduced) - E(oxidized) - E_{abs}(eff; she) \tag{2}$$

Here, E(reduced) and E(oxidized) are the total electrochemical potentials of the reduced and oxidized species, respectively. These values can be obtained from the total Gibbs Free energies (G) through Eq. (3).

$$G = -nFE \tag{3}$$

where n is the number of transferred electrons (typically $n = 1$) and F the Faraday constant. Owing to the removal of systematic errors resulting from the ambiguities related to the otherwise ambiguous choice of the absolute potential, this method is able to predict ET potentials with high accuracy [34].

The effective absolute potential can be connected to the energy of solvation of a proton through the hydrogen evolution reaction (Reaction 4)

$$H^+ + e^- \rightarrow 0.5H_2, \; E^o = 0V \tag{4}$$

Assuming a pH of 0 and the use of the she scale, the effective proton solvation energy, $G_{eff}(H^+)$, is given by

$$G_{eff}(H^+) = 0.5G(H_2) - \frac{E_{abs}(eff; she)}{nF}. \tag{5}$$

$G(H_2)$ corresponds to the total energy of hydrogen. $G_{eff}(H^+)$ can be used to accurately compute the Gibbs Free energy of acid-base reactions and thus, their pK_a values.

CVs were simulated in the DigiElch software (Gamry) based on data from the DFT calculations. Butler Volmer kinetics were used in the simulation with a fast heterogeneous rate constant, k_s, of 1 cms^{-1} for all electron transfer reactions. The scan rate was set to 100 mV s^{-1} and the forward rate constant, k_f, for protonation equilibria to 10^9 s^{-1} [36]. The diffusion coefficient, D, was set to $2 \cdot 10^{-6}$ cm^2 s^{-1} for all 2X-NDI species [13] and $1 \cdot 10^{-5}$ cm^2 s^{-1} for the proton. The concentration of 2X-NDI was 1 mM.

3. Results and discussion

Experimental results have shown that NDI can be reduced in two electron transfer steps in aqueous solution [13]. Thus, only the addition of the first two electrons was handled computationally. In the following sections, an electron transfer reaction is denoted "E", and a chemical reaction step – protonation in this context – is denoted "C".

3.1. Computational electrochemical results

In Fig. 2, the scheme of squares system for 2X-NDI is shown, and the corresponding computationally acquired reduction potentials and pK_a values are presented in Table 1. It should be noted that in Fig. 2, reductions and protonations are depicted on the oxygen atoms diagonally opposite to each other, although, as shown in Table 5, this is not necessarily the case.

For all the investigated structures, the protonated radical, 2X-NDIH[•], is largely unattainable across the aqueous pH range, as seen by the negative pK_{a2} values. Thus, in systems where E_1 is more

Table 1
Potentials and pKa-values for the different NDI species.

X	E_1	E_2	E_3	E_4	E_5	E_6	pK_{a1}	pK_{a2}	pK_{a3}	pK_{a4}	pK_{a5}	pK_{a6}
H	−0.20	−0.58	0.39	−0.09	0.87	0.48	−15.48	−5.44	2.90	−17.28	−9.21	0.45
Br	−0.04	−0.48	0.54	0.02	1.09	0.55	−16.16	−6.47	1.98	−19.62	−10.30	−1.28
F	−0.05	−0.49	0.53	0.01	0.98	0.56	−16.60	−6.73	1.78	−18.01	−10.48	−1.25
CN	0.31	−0.15	0.77	0.38	1.27	0.83	−17.24	−9.62	−0.55	−19.86	−11.31	−3.84
OH	−0.19	−0.59	0.36	−0.09	0.75	0.41	−15.95	−6.72	1.85	−17.16	−10.50	−2.14
NO_2	0.34	−0.04	0.90	0.51	1.32	1.13	−19.60	−10.50	−1.90	−20.38	−13.29	−2.88
OMe	−0.15	−0.60	0.39	−0.26	0.70	0.34	−11.95	−2.73	3.00	−15.74	−10.42	−0.35
NH_2	−0.60	−0.90	−0.23	−0.38	0.48	−0.10	−7.27	−0.93	7.70	−13.71	−1.77	3.07
NH_2-H^+	−0.12	−0.54	0.34	−0.08	0.91	0.29	−13.72	−5.93	1.92	−17.64	−8.07	−1.87
NH_2−$2H^+$	0.35	−0.08	0.91	0.46	1.40	1.01	−19.78	−10.38	−1.28	−23.48	−15.12	−5.79
DMA	−0.55	−0.74	0.02	−0.29	0.45	0.23	−13.48	−3.89	3.68	−14.73	−7.44	1.50
DMA-H^+	−0.13	−0.47	0.27	−0.03	0.81	0.38	−12.82	−6.05	1.51	−19.19	−10.12	−3.22
DMA-$2H^+$	0.35	−0.11	0.95	0.38	1.39	0.88	−20.60	−10.36	−2.07	−21.98	−14.68	−6.14

Potentials are referenced vs SHE.
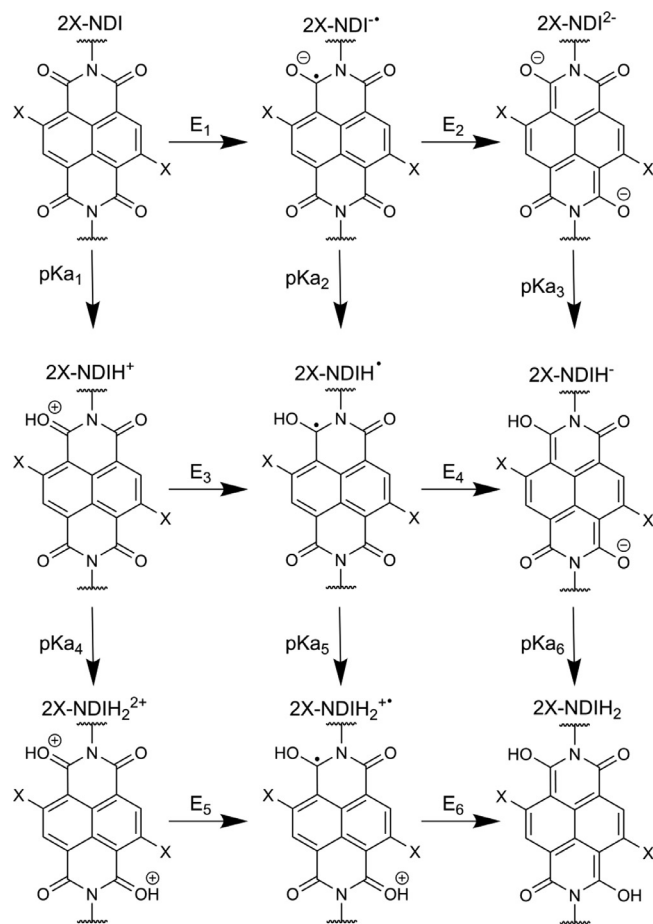
Fig. 2. Scheme of squares for 2X-NDI.

positive than E_2, a cyclic voltammogram starting from $E > E_1$, going in the negative direction can be predicted to display two separate redox couples. The first redox couple will be pH-independent for all these species due to the negative value of pK_{a2}. The second redox couple, however, will display a pH-dependence at pH < pK_{a3} due to the coupling of a proton with the second electron transfer. If, however, pK_{a3} is significantly below 0, no pH-dependence will be seen, such as for 2CN-NDI and 2NO$_2$-NDI, see Table 1.

For the two core-aminated species, 2NH$_2$-NDI and 2DMA-NDI, the scheme of squares has 27 components instead of 9 because each of the nine species that is unprotonated on the core-amines is in equilibrium with its mono- and di-protonated analogue. How-

ever, based on the negative values of pK_{a1}, pK_{a4} and pK_{a5}, the equilibria involving the three species in the lower left corner of the scheme in Fig. 2 can be disregarded. The pKa values governing the remaining equilibria are shown in Table 2 for 2NH$_2$-NDI and Table 3 for 2DMA-NDI. The analysis of the core-aminated species is presented in Section 3.1.3

3.1.1. Reduction mechanism and protonation

As previously stated, 2X-NDI can be reduced with one or two electrons and protonated once or twice, as shown in the scheme of squares in Fig. 2. The singly reduced 2X-NDI generally remains in the deprotonated radical anion form, 2X-NDI$^{-\bullet}$, as protonation would hamper charge and radical delocalization.

If 2X-NDI is reduced with two electrons at pH > pK_{a3} and pK_{a6}, the fully reduced form will stay deprotonated in the dianionic form, 2X-NDI^{2-}. If instead, the reduction is performed at a pH value below pK_{a3} but above pK_{a6}, the 2X-NDIH$^-$ form will predominate, for which two different 2X-NDIH$^-$ tautomers exist, and these were studied for all the investigated species with DFT. For 2X-NDIH$^-$, the delocalization of the negative charge is shared by the two oxygen atoms opposite to the protonated one. Based on the free energies of the optimized structures, their distributions among the different forms were calculated, see Table 4. The most energetically favorable form for each structure was used for further analysis. Surprisingly, no correlation between the electronegativity of the substituent and the preferred form could be seen.

Similarly, after a two-electron reduction when pH < pK_{a6}, the doubly protonated fully reduced form, 2X-NDIH$_2$ is acquired, and three tautomers exist, see Table 5, for which the relative Gibbs free energies are found in Section 6 in the SI. 2CN-NDI was excluded from the tables since pK_{a3} and pK_{a6} have negative values, see Table 1.

Interestingly, most 2X-NDIH$_2$ species seem to have Form 2 as a preferred arrangement. As 2X-NDIH$_2$ lacks the resonance stabilization that its deprotonated form has, the electrostatic interactions between the hydroxyl groups and the substituents should play a relatively large role. Therefore, the hydroxyl groups should tend to be either close to, or far away from the substituents. However, the most polarized configuration, Form 2, is generally seen, with the only deviation observed for the strongly electron-donating NH$_2$ groups, which instead tend towards Form 3. Looking at Form 1, hydrogen bonding between the hydroxyl group and electron-rich groups such as NH$_2$ was expected to decrease the energy for the structure, but instead, Form 1 is energetically disfavored for all substituents.

3.1.2. Cyclic voltammetry simulations – non-core-aminated species

CVs for the 2X-NDI species were simulated at different pH values, as shown for 2H-NDI and 2Br-NDI in Fig. 3, with
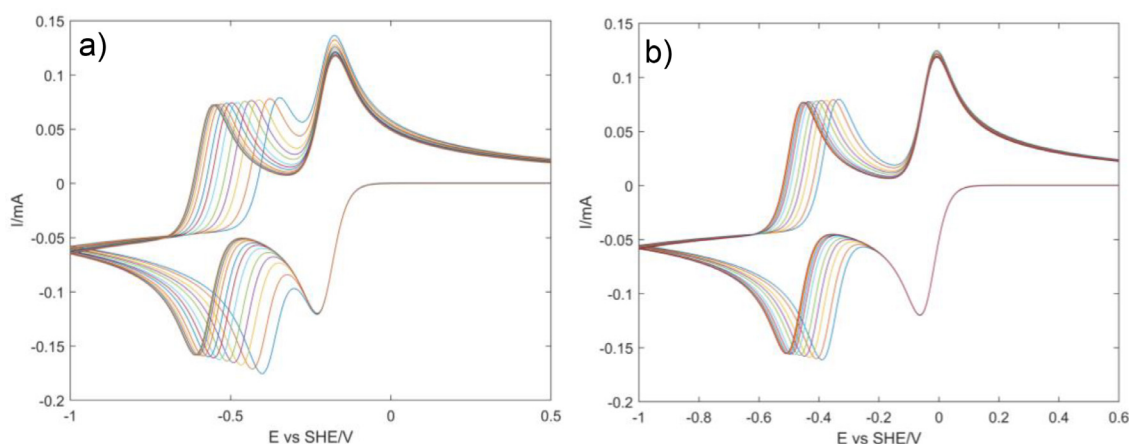
Table 2
pKa values for amine protonation equilibria for the components of the scheme of squares for 2NH2-NDI.

2NH2-NDI	2NH2-NDI−•	2NH2-NDIH•	2NH2-NDI2−	2NH2-NDIH−	2NH2-NDIH2
−7.3	0.9	−4.1	6.9	1.1	−3.8
NH2/NH3+-NDI	NH2/NH3+-NDI−•	NH2/NH3+-NDIH•	NH2/NH3+-NDI2−	NH2/NH3+-NDIH−	NH2/NH3+-NDIH2
−11.6	−3.6	−8.1	4.2	1.0	−2.9
2NH3+-NDI	2NH3+-NDI−•	2NH3+-NDIH•	2NH3+-NDI2−	2NH3+-NDIH−	2NH3+-NDIH2

Table 3
pKa values for amine protonation equilibria for the components of the scheme of squares for 2DMA-NDI.

2DMA-NDI	2DMA-NDI−•	2DMA-NDIH•	2DMA-NDI2−	2DMA-NDIH−	2DMA-NDIH2
1.7	8.8	6.7	13.4	11.2	6.4
DMA/DMAH+-NDI	DMA/DMAH+-NDI−•	DMA/DMAH+-NDIH•	DMA/DMAH+-NDI2−	DMA/DMAH+-NDIH−	DMA/DMAH+-NDIH2
−2.1	6.0	1.7	12.1	8.5	5.6
2DMAH+-NDI	2DMAH+-NDI−•	2DMAH+-NDIH•	2DMAH+-NDI2−	2DMAH+-NDIH−	2DMAH+-NDIH2

Fig. 3. Simulated CVs at various pH for a) 2H-NDI, pH 0–7, b) 2Br-NDI, pH 0–7. The pH increases to the left.

Table 4
Distributions between the two tautomeric forms of the mono-protonated fully reduced species, 2X-NDIH−.

X	Form 1	Form 2
H*		100.00%
Br	79%	21%
F	32%	68%
OH	1%	99%
OMe	22%	78%
NH2	100%	0%

* Form 1 and Form 2 are identical for 2H-NDI.

Table 5
Distributions between the three tautomeric forms of the di-protonated fully reduced species, 2X-NDIH2.

X	Form 1	Form 2	Form 3
H*	2%	96%	2%
Br	4%	95%	1%
F	3%	94%	3%
OH	0%	75%	25%
OMe	1%	82%	16%
NH2	0%	9%	91%

* Form 1 and Form 3 are identical for 2H-NDI.

accompanying potential – pH diagrams in Fig. 4. Corresponding graphs for the remaining 2X-NDI species are presented in Section 2 in the SI. The pH-dependence for the hydrogen evolution reaction (HER) is included in the potential – pH diagrams to illustrate the possible interference between the reduction of NDI and the reduction of protons or water.

All investigated non-core-aminated molecules exhibit two separate redox couples, revealing a high stability of the formed radical anion state, 2X-NDI−•. The expected pH-independence for the first electron is seen due to the negative pK_{a2} values of all the investigated molecules. From the CV simulations, electrode surface concentrations of the produced species during the potential sweep were extracted and used to help determine the reduction/oxidation mechanisms at each pH. Surface concentrations as well as the main

reductive/oxidative pathway for each species at selected pH values, are given in Sections 3 and 4 in the SI.

At pH values exceeding 7, none of the two-electron reductions are accompanied by protons. At low pH values, however, on NDI di-substituted with H, Br or F both oxygen atoms are protonated, while with OH or OMe only one oxygen is protonated. 2CN-NDI and 2NO2-NDI remain unprotonated throughout the investigated pH-range.

3.1.3. Cyclic voltammetry simulations – core-aminated species

The core-aminated species were simulated with a larger set of reactions since protonation equilibria for the core-amines needed to be included as well, thus expanding the scheme of squares, see Tables 2,3 and Fig. 5.
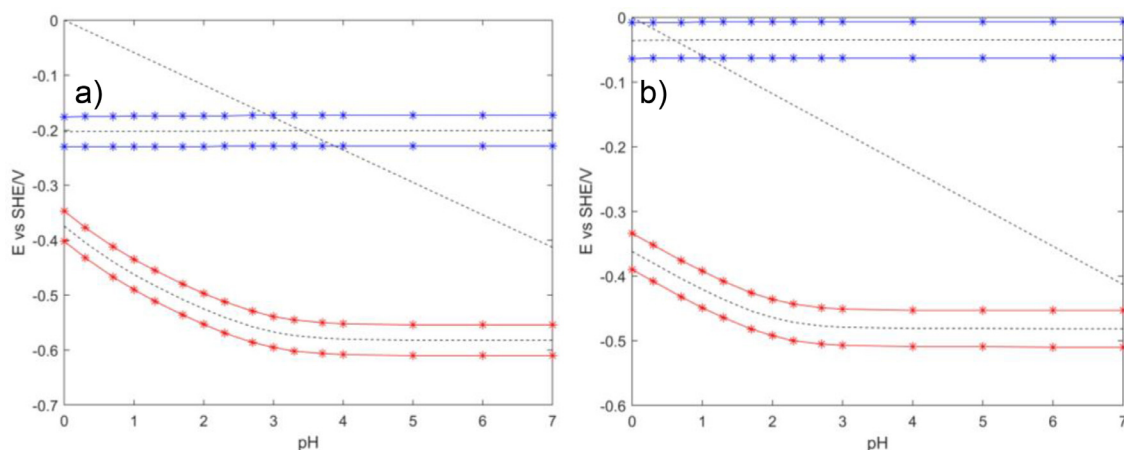
Fig. 4. Simulated potential – pH dependence of a) 2H-NDI and b) 2Br-NDI. The blue and red markers represent the anodic and cathodic peak potentials for the first and second electron transfers respectively. The diagonal dashed black line indicates the potential for the HER. (For interpretation of the references to colour in this figure legend, the reader is referred to the web version of this article.)
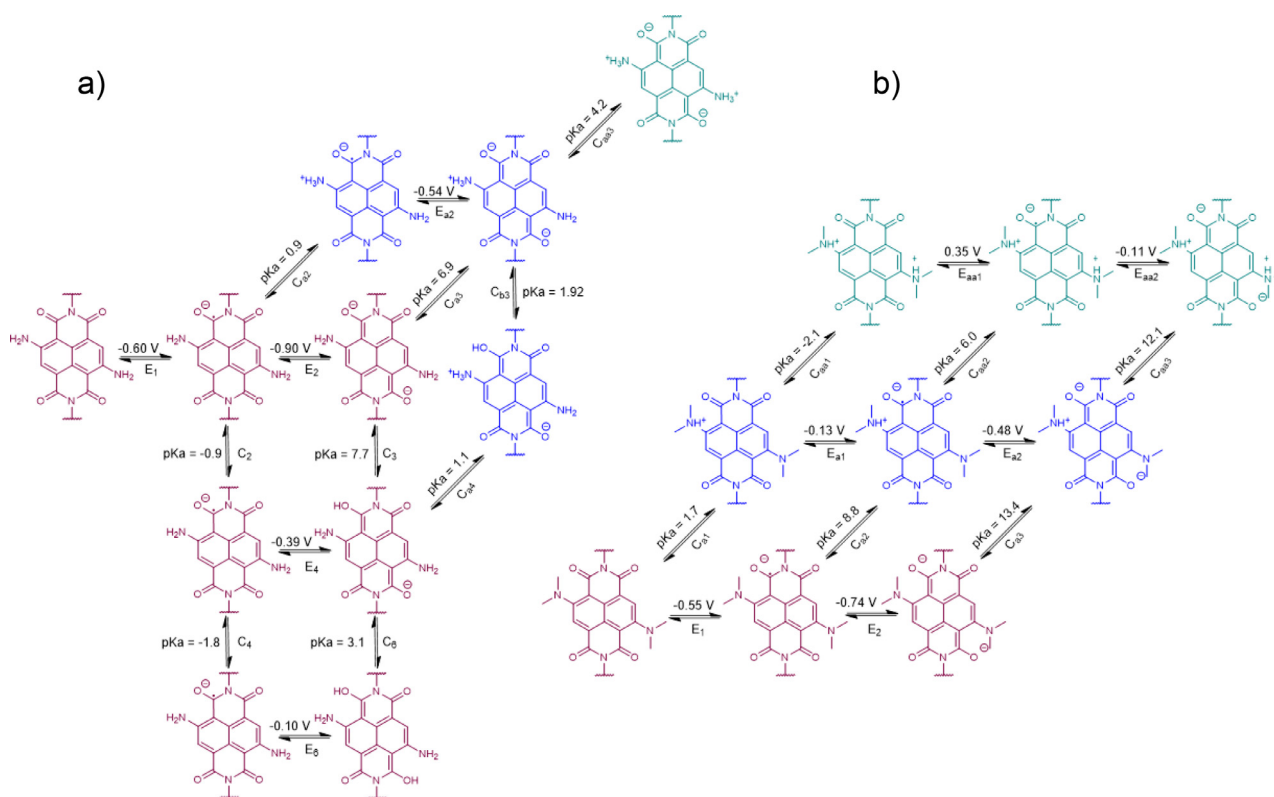

Fig. 5. Reactions included in the CV simulation of a) $2NH_2$-NDI and b) 2DMA-NDI.

Generally, a protonation reaction was included if its pK_a value was above −2, but sometimes, in order to reduce system complexity, an equilibrium with a relatively high pK_a value was excluded because it had a relatively much lower pK_a value than a competing equilibrium. The simulated CVs for $2NH_2$-NDI and 2DMA-NDI are shown in Fig. 6 and their potential – pH dependencies in Fig. 7.

$2NH_2$-NDI has only one redox couple at low pH values because the first electron transfer is immediately followed by a protonation on the core amine, which has a pK_a value of 0.9, see Fig. 5a, reaction C_{a2}. The formed protonated radical, $2NH_2(H^+)$-NDI$^{-•}$, is reduced at a more positive potential than that for the first electron transfer and only one peak is observed. This behavior is seen even at pH values considerably exceeding the pK_a value of 0.9, and this is due to the consumption of the protonated species,

$2NH_2(H^+)$-NDI$^{-•}$, that are reduced when formed, and the equilibrium is driven towards further protonation. In Fig. 8, surface concentrations for the reduction of $2NH_2$-NDI at selected pH values are shown. At pH 0 and potentials below −0.5 V, most of the reduced species occur in the core-protonated form, $2NH_2(2H^+)$-NDI^{2-}, but a smaller amount of $2NH_2$-NDIH$_2$ is seen as well. Due to the negative reduction potential of the radical anion, $2NH_2$-NDI$^{-•}$, see E_2 in Fig. 5a, $2NH_2$-NDIH$_2$ is formed either through the convoluted $E_1C_{a2}E_{a2}C_{b3}C_{a4}C_6$ pathway or through the $E_1C_2E_4C_6$ pathway. At pH 3, the surface concentration distribution is largely the same as at pH 0 with the exception of the occurrence of $2NH_2$-NDIH$^-$ and that some anion radicals, $2NH_2$-NDI$^{-•}$, persist instead of being protonated on the core amine. Further increasing the pH to 7 and above yields two separate redox couples with decreasing
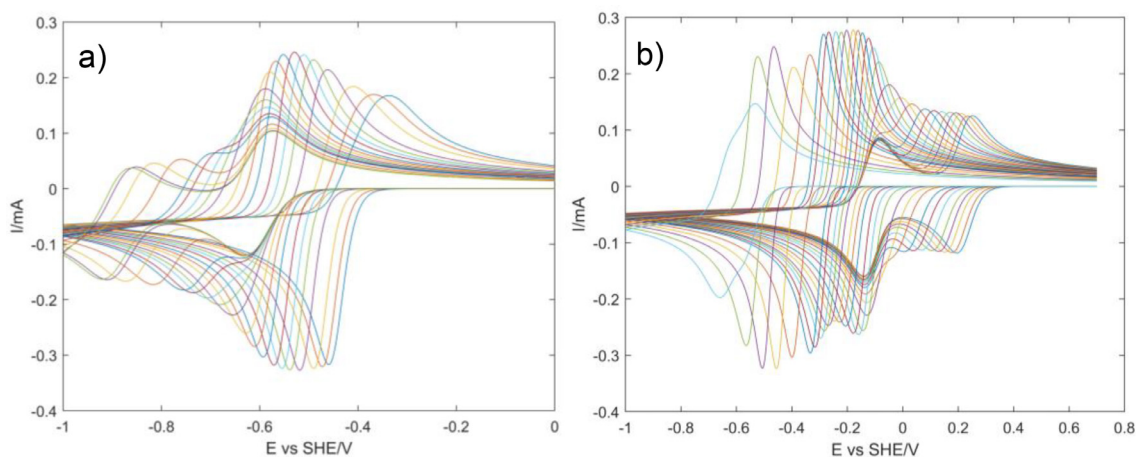
Fig. 6. Simulated CVs at various pH for the two core-aminated species. pH increases to the left. a) 2NH$_2$-NDI, pH 0–9, b) 2DMA-NDI, pH 0–12.
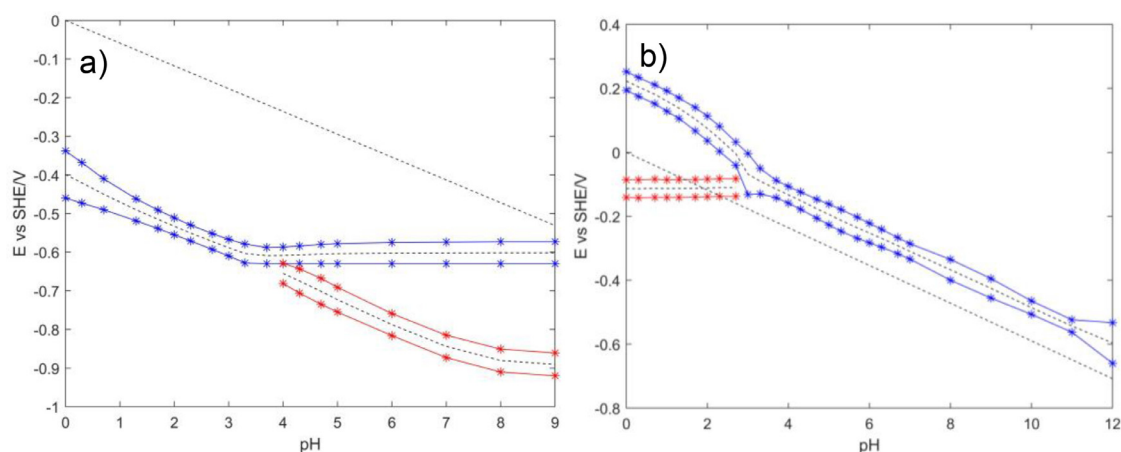
Fig. 7. Simulated potential – pH dependence of a) 2NH$_2$-NDI and b) 2DMA-NDI. The blue and red markers represent the anodic and cathodic peak potentials for the first and second electron transfers respectively. The diagonal dashed black line indicates the potential for the HER. (For interpretation of the references to colour in this figure legend, the reader is referred to the web version of this article.)
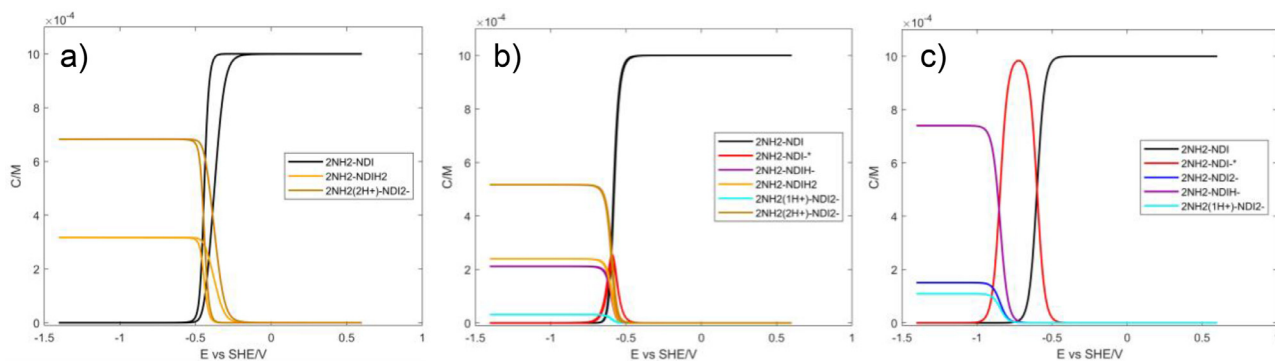
Fig. 8. Surface concentrations for 2NH$_2$-NDI at a) pH 0, b) pH 3 and c) pH 7.

pH-dependence at increasing pH that reach a separation of roughly 0.3 V at pH 9, see Fig. 7a.

For 2DMA-NDI, the dimethylamine substituents are more basic than the primary amines on 2NH$_2$-NDI and the molecule is therefore more readily protonated on the core than on the oxygen atoms. The potential-pH dependence of 2DMA-NDI is mirrored to that of 2NH$_2$-NDI, where at low pH, two redox couples occur, and merge at pH values above 3, see Fig. 7b. At pH 0, the first peak at 0.22 V has a potential expected of a concerted E$_{a1}$C$_{aa2}$ reaction through $\Delta G = -RT\ln K$ and Eq. (3), yielding $E =$

$-0.13\ V + \frac{RT\ln(10^{-6.0})}{-nF}$. The second electron transfer has a reduction potential of -0.11 V corresponding to E$_{aa2}$. At pH 3, the starting material is the fully deprotonated species and the C$_{a1}$E$_{a1}$C$_{aa2}$E$_{aa2}$ pathway is seen, based on the reduction potential, see Fig. 5b. At neutral pH, the reaction follows E$_1$C$_{a2}$E$_{a2}$C$_{aa3}$ with only the starting material and zwitterionic 2DMA(2H$^+$)-NDI^{2-} occurring in any appreciable amounts (Fig. 9). This is the selected pathway up to pH 10, after which eventually the peak starts dividing into two, as core-deprotonated species occur at pH above 12. However, 2DMA-NDI was found experimentally to rapidly decompose at pH values
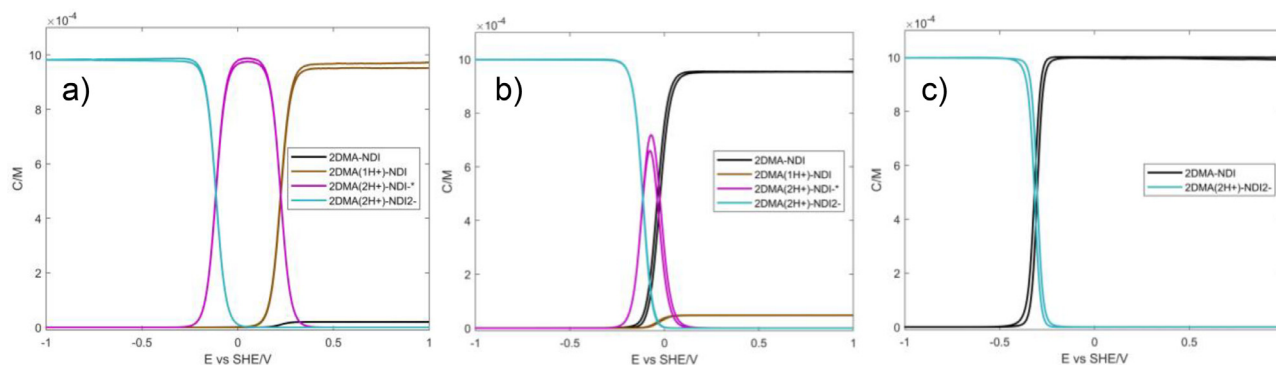
Fig. 9. Surface concentrations for 2DMA-NDI at a) pH 0, b) pH 3 and c) pH 7.
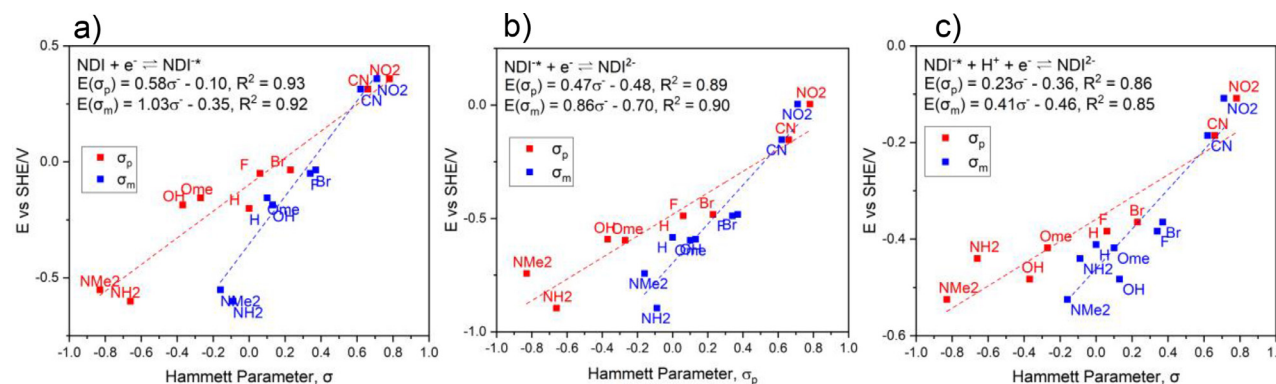

Fig. 10. Hammett correlations for the a) E_1, b) E_2 and c) E_2C_3 reduction pathways.

exceeding 12 and this behavior is therefore unlikely to be possible to observe experimentally.

3.1.4. Hammett parameters

In order to establish a structure-property relationship for the 2X-NDI species, an analysis using Hammett parameters was done. Hammett parameters can be used to gage the sensitivity, ρ, of a system to electron-withdrawing and electron-donating substituents [37]. Fig. 10a and b show how the computationally acquired reduction potentials of 2X-NDI vary with substituent for the two electron transfers unaccompanied by protons. Fig. 10c shows the correlation for the concerted E_2C_3 reaction from the radical anion, 2X-NDI$^{-\bullet}$. There are different types of Hammett parameters [38] based on the nature of the interaction, as well as the position of the substituent. σ_p^- and σ_p^+ are used if resonance effects are expected to come into play, whereas σ_m and σ_p are used for substituents meta and para to the investigated part of the molecule, historically the carboxylic group on benzoic acid [38].

The potentials correlate well with the σ_m and σ_p parameters as seen in Fig. 10, but not as well for the σ_p^- and σ_p^+ set, with the exception of σ_p^- for E_2C_3. This is an indication that the substituent effect on NDI is mainly inductive in nature, perhaps as a consequence of the naphthalene core and the imides being cross-conjugated. Hammett correlation data is given in Section 7 in the SI.

On the investigated 2X-NDI species, the substituents are in the diagonally opposite 2,6-positions, and the para-position for the one side will correspond to the meta-position for the other. Therefore, it is reasonable that the correlations between the potentials are equally good for both the σ_m and σ_p parameter sets. The correlation parameters allow for a fast first prediction of reduction potentials for other substituents than those included in this work sim-

ply by inserting their Hammett parameters in the formulae given in Fig. 10.

3.2. Experimental electrochemical results

CVs for 2H-NDI, 2Br-NDI and 2DMA-NDI at different pH values are shown in Fig. 11 and their potential – pH diagrams in Fig. 12.

Qualitatively, the redox behavior of both 2H-NDI and 2Br-NDI show good agreement with DFT results. The first, more positive, electron transfer is independent of pH in the investigated range while the potential for the second electron transfer decreases by 120 mV between pH 0 and pH 1 for 2H-NDI and 100 mV for 2Br-NDI, roughly corresponding to 1e$^-$/2H$^+$. This number decreases gradually until the second electron transfer becomes pH-independent above approximately pH 3.5 for 2H-NDI and pH 4 for 2Br-NDI. From the DFT results, as was seen in Fig. 3, the potentials decrease by 88 mV for 2H-NDI and 59 mV for 2Br-NDI between pH 0 and pH 1 and then become independent of pH at around pH 4 for 2H-NDI and pH 3 for 2Br-NDI, which correspond to their respective pK_{a6} values. The higher experimental value of the potential – pH slope at low pH values indicates that the calculated pK_{a3} value was slightly underestimated for both species. The point where the second electron becomes pH-independent, however, was estimated quite accurately, and the calculated pK_{a6} values for 2H-NDI and 2Br-NDI are quite close to true. The calculated pK_{a3} and pK_{a6} values were 2.9 and 0.5 for 2H-NDI and 2.0 and -1.3 2Br-NDI respectively, see Table 1.

2DMA-NDI only has one peak in the investigated pH range, in contrast to the simulations which predicted two redox couples at low pH. The difference is caused by an underestimation of E_{aa2} and/or an overestimation of E_{a1} and the pK_a for C_{aa2}. At low pH, the potential-pH slope is close to 30 mV, indicating a 2e$^-$/1H$^+$
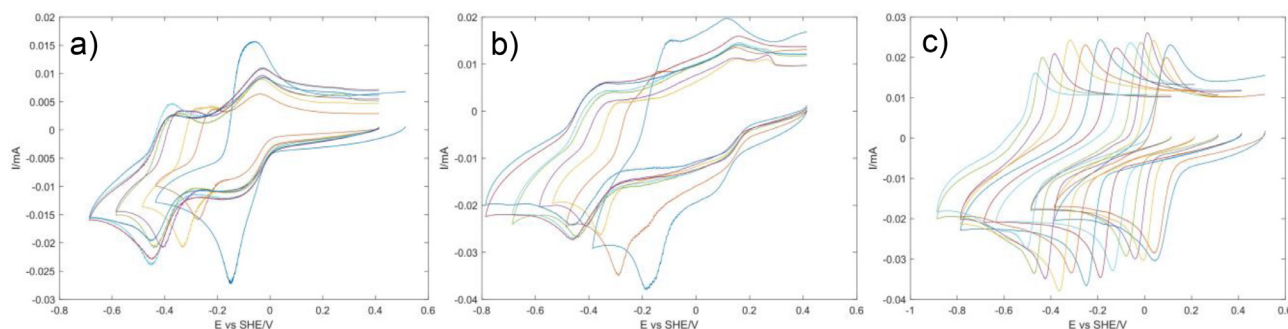
Fig. 11. Variation of CVs with pH for 1 mM a) 2H-NDI, pH 0–7, b) 2Br-NDI, pH 0–7 and c) 2DMA-NDI, pH 0–12. Sweep rate: 100 mV s^{-1}. The pH increases to the left.
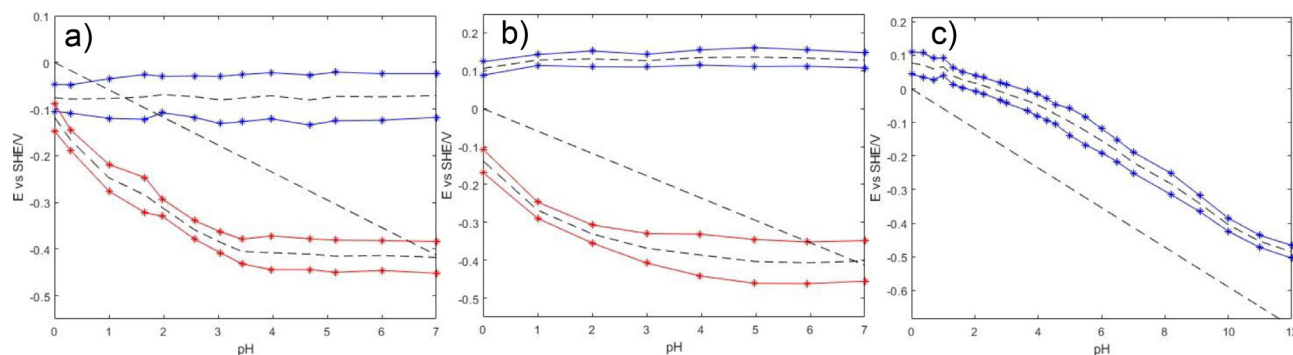
Fig. 12. Potential – pH dependence on the experimentally investigated NDI species at a concentration of 1 mM. a) 2H-NDI, b) 2Br-NDI and c) 2DMA-NDI. The blue and red markers represent the anodic and cathodic peak potentials for the first and second electron transfers respectively. The dashed black line indicates the potential for the HER. (For interpretation of the references to colour in this figure legend, the reader is referred to the web version of this article.)

mechanism but, interestingly, at pH values above roughly 4.5, the slope increases to 60 mV or 2e$^-$/2H$^+$. Looking at the simulated surface concentrations of 2DMA-NDI during a CV, see Fig. 7, it is seen that one proton is acquired at pH 0, and two protons at pH 3 and above, showing good correlation between the simulations and experiments. The unconventional behavior of the redox reaction including a higher number of protons at higher pH values is thus explained by the starting material existing in its protonated form at lower pH values.

Experimental pK$_a$ values of 2DMA-NDI were acquired by collecting ^{1}H NMR spectra at a series of varying pH values. The sidechain amine was found to have a pK$_a$ value of 9.15, which is comparable to results from a previously reported potentiometric titration of 2H-NDI [13]. In that experiment, however, 2H-NDI was found to precipitate out of solution at pH 8.1 due to the deprotonated species being of neutral charge, so no pK$_a$ value could be acquired. For 2DMA-NDI, only one of the core-dimethylamines was found to be possible to protonate in the aqueous pH range, with pK$_a$ = 3.95 - roughly two units higher than was predicted by DFT calculations. The size of this error is in line with the current level of accuracy that can be achieved by DFT-based pK$_a$ predictions. The pK$_a$ value for protonating the second amine was predicted to be −2.1, which is supported by the NMR titration data for which more information can be found in Section 8 in the SI.

3.3. Applicability for redox flow batteries

In order to have electrochemical properties that enable use in AORFBs, a molecule needs to have reversible electron transfers at as negative potentials as possible without incurring efficiency losses due to hydrogen evolution. Many of the examined molecules have a declining pH-dependence at increasing pH, allowing for the position of the potential in relationship to the HER to be tuned by

Table 6
Calculated reduction potentials at pH 0 and pH 7 for 2X-NDI.

	E vs SHE (V) - pH 0			E vs SHE (V) - pH 7		
X	1st e$^-$	2nd e$^-$	Average	1st e$^-$	2nd e$^-$	Average
H	−0.20	−0.38	−0.29	*−0.20*	*−0.58*	*−0.39*
Br	−0.04	−0.36	−0.20	−0.04	−0.48	−0.26
F	−0.05	−0.38	−0.22	−0.05	−0.49	−0.27
CN	0.31	−0.15	0.08	0.31	−0.15	0.08
OH	−0.19	−0.48	−0.33	−0.19	−0.59	−0.39
NO$_2$	0.36	0.01	0.18	0.34	−0.04	0.15
OMe	−0.16	−0.41	−0.28	−0.15	−0.60	−0.38
2NH$_2$-NDI	−0.40	−0.40	−0.40	−0.60	−0.84	−0.72
2DMA-NDI	0.22	−0.11	0.05	−0.31	−0.31	−0.31

changing the pH. The molecules in the negative electrolyte are reduced upon charging in a full cell redox flow battery (RFB) system. Therefore, the HER constrains the rate at which the battery can be charged, as higher overpotentials will result in a larger portion of hydrogen being evolved, and a decrease in coulombic efficiency. However, the carbonaceous materials used as electrodes in RFBs are poor electrocatalysts for hydrogen evolution, and therefore, the thermodynamic potential of the HER can often be surpassed significantly without suffering from the parasitic reaction [9,39,40].

The reduction potentials acquired from the CV simulations at pH 0 and pH 7 are shown in Table 6. Comparing the experimental results presented in Fig. 12 to the computational results in Table 6, it can be seen that the reduction potentials for 2H-NDI and 2Br-NDI were predicted 120–200 mV more negative than found experimentally. The calculated potential for 2DMA-NDI was only 27 mV lower than the experimental value at pH 0, and 90 mV lower than found at pH 7. Therefore, the influence of the HER in a redox flow battery application might be less than what would be predicted from the presented potentials obtained by DFT calculations.

Nonetheless, a higher coulombic efficiency due to a decreased impact of the HER would be expected at either pH 0 or pH 7 compared to the values in between.

Looking at using 2X-NDI in the negative electrolyte, the non-aminated molecules would yield two potential plateaus in a galvanostatic charge experiment, while 2DMA-NDI and 2NH$_2$-NDI would yield one or two plateaus depending on the pH. Consequently, in the conditions where two plateaus are observed, the first half of the capacity would be possible to charge with a large applied overpotential and a high charging rate, while the second would need to take longer in order to avoid the HER. Depending on the application, the ability to fast-charge part of the capacity could be beneficial.

The calculated reduction potential of 2NH$_2$-NDI is between 300 and 400 mV more negative than that of the HER throughout the pH range, which likely makes its reduction too negative to access in a battery configuration. However, if the potential was underestimated in the calculations, as was the case for 2H-NDI and 2Br-NDI, the negative potential of 2NH$_2$-NDI could make it an interesting candidate and an experimental assessment would be justified, if a viable synthesis route can be found. 2CN-NDI and 2NO$_2$-NDI could find application in the positive electrolyte, especially if their potentials share the underestimation that was seen for the two synthesized non-aminated molecules.

The average value of the potentials was taken in order to compare the molecules. 2H-NDI, 2OH-NDI, 2OMe-NDI, 2DMA-NDI and 2NH$_2$-NDI have reduction potentials that would merit experimental investigation.

In the case of a symmetric redox flow battery that uses the same molecule in both the negative and positive electrolyte, a large potential difference between the first and the second electron is desired. No molecule in the studied set shows a separation of more than 0.5 V, which would be needed for expedient application in a symmetric AORFB setup.

4. Conclusion

The electrochemistry of nine NDI molecules, differentiated by their core-functionalization, have been studied computationally, and three of them experimentally. A comprehensive selection of thermodynamic data was acquired from DFT-calculations and used to simulate CVs and gain mechanistic insight into the redox behavior of the molecules. Most of the species were characterized by having a first pH-independent electron transfer followed by a second electron transfer that was pH-dependent at low pH to gradually become pH-independent with increasing pH. The exception was the two core-aminated molecules which had a more complex redox behavior, on which the results from the simulations were decisive. 2DMA-NDI showed a counterintuitive lower pH-dependence at lower pH, which was attributed to the core-protonation of the starting material. ^{1}H NMR spectroscopy was used to determine the pK$_a$ of 2DMA-NDI and it was found that the sidechain dimethylamine group has a pK$_a$ of 9.15 and the core dimethylamine group could only accept one proton with a pK$_a$ of 3.95.

A structure-property relationship for the 2X-NDI species were established using Hammett parameters, ρ. Linear dependencies were obtained between the reduction potential for the first and second electron transfer, respectively, and σ_m and σ_p. These correlations allow for a first prediction of reduction potentials for other substituents than those included in this work.

2H-NDI, 2OH-NDI, 2OMe-NDI, 2NH$_2$-NDI and 2DMA-NDI were identified as potential RFB candidates, out of which 2H-NDI and 2DMA-NDI are currently being studied in redox flow batteries by this group.

Declaration of Competing Interest

The authors declare that they have no known competing financial interests or personal relationships that could have appeared to influence the work reported in this paper.

Credit authorship contribution statement

Cedrik Wiberg: Conceptualization, Formal analysis, Investigation, Writing - original draft. **Michael Busch:** Investigation, Writing - review & editing. **Lars Evenäs:** Writing - review & editing, Supervision. **Elisabet Ahlberg:** Conceptualization, Formal analysis, Writing - review & editing, Supervision.

Supplementary materials

Supplementary material associated with this article can be found, in the online version, at doi:10.1016/j.electacta.2020.137480.

References

[1] S. Gentil, D. Reynard, H.H. Girault, Aqueous organic and redox-mediated redox flow batteries: a review, Curr. Opin. Electrochem. 21 (2020) 7–13 https://doi.org/, doi:10.1016/j.coelec.2019.12.006.

[2] R. Chen, Redox flow batteries for energy storage: recent advances in using organic active materials, Curr. Opin. Electrochem. 21 (2020) 40–45 https://doi.org/, doi:10.1016/j.coelec.2020.01.003.

[3] F. Zhong, M. Yang, M. Ding, C. Jia, Organic electroactive molecule-based electrolytes for redox flow batteries: status and challenges of molecular design, Front. Chem. 8 (2020) https://doi.org/, doi:10.3389/fchem.2020.00451.

[4] D.P. Tabor, R. Gómez-Bombarelli, L. Tong, R.G. Gordon, M.J. Aziz, A. Aspuru-Guzik, Mapping the frontiers of quinone stability in aqueous media: implications for organic aqueous redox flow batteries, J. Mater. Chem. A 7 (2019) 12833–12841 https://doi.org/, doi:10.1039/c9ta03219c.

[5] R. Ye, D. Henkensmeier, S.J. Yoon, Z. Huang, D.K. Kim, Z. Chang, S. Kim, R. Chen, Redox flow batteries for energy storage: a technology review, J. Electrochem. Energy Convers. Storage 15 (2017) 010801 https://doi.org/, doi:10.1115/1.4037248.

[6] W. Liu, W. Lu, H. Zhang, X. Li, Aqueous flow batteries: research and development, Chem. – Eur. J. 25 (2019) 1649–1664 https://doi.org/, doi:10.1002/chem.201802798.

[7] K. Wedege, E. Drazevic, D. Konya, A. Bentien, Organic redox species in aqueous flow batteries: redox potentials, chemical stability and solubility, Sci. Rep. 6 (2016) 39101 https://doi.org/, doi:10.1038/srep39101.

[8] Y. Ji, M.A. Goulet, D.A. Pollack, D.G. Kwabi, S. Jin, D. Porcellinis, E.F. Kerr, R.G. Gordon, M.J. Aziz, A phosphonate-functionalized quinone redox flow battery at near-neutral ph with record capacity retention rate, Adv. Energy Mater. 9 (2019) 1900039–1900046 https://doi.org/, doi:10.1002/aenm.201900039.

[9] J. Luo, W. Wu, C. Debruler, B. Hu, M. Hu, T.L. Liu, A 1.51 v pH neutral redox flow battery towards scalable energy storage, J. Mater. Chem. A 7 (2019) 9130–9136 https://doi.org/, doi:10.1039/c9ta01469a.

[10] C. Wiberg, T.J. Carney, F. Brushett, E. Ahlberg, E. Wang, Dimerization of 9,10-anthraquinone-2,7-disulfonic acid (AQDS), Electrochim. Acta 317 (2019) 478–485 https://doi.org/, doi:10.1016/j.electacta.2019.05.134.

[11] T.J. Carney, S.J. Collins, J.S. Moore, F.R. Brushett, Concentration-dependent dimerization of anthraquinone disulfonic acid and its impact on charge storage, Chem. Mater. 29 (2017) 4801–4810 https://doi.org/, doi:10.1021/acs.chemmater.7b00616.

[12] M.-.A. Goulet, M.J. Aziz, Flow battery molecular reactant stability determined by symmetric cell cycling methods, J. Electrochem. Soc. 165 (2018) A1466–A1477 https://doi.org/, doi:10.1149/2.0891807jes.

[13] C. Wiberg, F. Owusu, E. Wang, E. Ahlberg, Electrochemical evaluation of a napthalene diimide derivative for potential application in aqueous organic redox flow batteries, Energy Technol. 7 (2019) https://doi.org/, doi:10.1002/ente.201900843.

[14] S.V. Bhosale, C.H. Jani, S.J. Langford, Chemistry of naphthalene diimides, Chem. Soc. Rev. 37 (2008) 331–342 https://doi.org/, doi:10.1039/B615857A.

[15] G.S. Vadehra, R.P. Maloney, M.A. Garcia-Garibay, B. Dunn, Naphthalene diimide based materials with adjustable redox potentials: evaluation for organic lithium-ion batteries, Chem. Mater. 26 (2014) 7151–7157 https://doi.org/, doi:10.1021/cm503800r.

[16] P. Ledwon, D. Ovsiannikova, T. Jarosz, S. Gogoc, P. Nitschke, W. Domagala, In-sight into the properties and redox states of n-dopable conjugated polymers based on naphtalene diimide units, Electrochim. Acta 307 (2019) 525–535 https://doi.org/, doi:10.1016/j.electacta.2019.03.169.

[17] A.R. Smith, B. Iverson, Chapter 2 NDI as a DNA intercalator, naphthalenedi-imide and its congeners: from molecules to materials, R. Soc. Chem. (2017) 37–71 https://doi.org/, doi:10.1039/9781782621386-00037.

[18] C. Batchelor-McAuley, Q. Li, S.M. Dapin, R.G. Compton, Voltammetric charac-terization of DNA intercalators across the full pH range: anthraquinone-2,6-disulfonate and anthraquinone-2-sulfonate, J. Phys. Chem. B 114 (2010) 4094–4100 https://doi.org/, doi:10.1021/jp1008187.

[19] F. Doria, M. Nadai, G. Sattin, L. Pasotti, S.N. Richter, M. Freccero, Water soluble extended naphthalene diimides as pH fluorescent sensors and G-quadruplex ligands, Org. Biomol. Chem. 10 (2012) 3830–3840 https://doi.org/, doi:10.1039/c2ob07006e.

[20] Q. Lin, L. Liu, F. Zheng, P.-.P. Mao, J. Liu, Y.-.M. Zhang, H. Yao, T.-.B. Wei, A benzimidazole functionalized NDI derivative for recyclable fluorescent de-tection of cyanide in water, RSC Adv. 7 (2017) 38458–38462 https://doi.org/, doi:10.1039/C7RA07247C.

[21] C. Roger, F. Wurthner, Core-tetrasubstituted naphthalene diimides: synthesis, optical properties, and redox characteristics, J. Org. Chem. 72 (2007) 8070–8075 https://doi.org/, doi:10.1021/jo7015357.

[22] J. Shukla, P. Mukhopadhyay, Synthesis of functionalized naphthalene diimides and their redox properties, Eur. J. Org. Chem. (2019) (2019) 7770–7786 https://doi.org/, doi:10.1002/ejoc.201901390.

[23] Y. Shi, H. Tang, S. Jiang, L.V. Kayser, M. Li, F. Liu, F. Ji, D.J. Lipomi, S.P. Ong, Z. Chen, Understanding the electrochemical properties of naphthalene di-imide: implication for stable and high-rate lithium-ion battery electrodes, Chem. Mater. 30 (2018) 3508–3517 https://doi.org/, doi:10.1021/acs.chemmater.8b01304.

[24] L. Li, J. Wang, M. Chen, Y. Chen, W. Xiao, D. Chen, M. Lin, The impact of vertical π-extension on redox mechanisms of aromatic diimide dyes, Chin. Chem. Lett. 30 (2019) 2254–2258 https://doi.org/, doi:10.1016/j.cclet.2019.05.040.

[25] A.V. Mumyatov, A.F. Shestakov, N.N. Dremova, K.J. Stevenson, P.A. Troshin, New naphthalene-based polyimide as an environment-friendly organic cath-ode material for lithium batteries, Energy Technol. 7 (2019) https://doi.org/, doi:10.1002/ente.201801016.

[26] X. Wang, L. Chen, F. Lu, J. Liu, X. Chen, G. Shao, Boosting aqueous zn2+ storage in 1,4,5,8-naphthalenetetracarboxylic dianhydride through nitrogen substitu-tion, ChemElectroChem 6 (2019) 3644–3647 https://doi.org/, doi:10.1002/celc.201900750.

[27] V. Medabalmi, M. Sundararajan, V. Singh, M.-.H. Baik, H.R. Byon, Naphthalene diimide as a two-electron anolyte for aqueous and neutral pH redox flow bat-teries, J. Mater. Chem. A 8 (2020) 11218–11223 https://doi.org/, doi:10.1039/d0ta01160f.

[28] M. Zhou, Y. Chen, M. Salla, H. Zhang, X. Wang, S.R. Mothe, Q. Wang, Single-molecule redox-targeting reactions for a ph-neutral aqueous organic redox flow battery, Angew. Chem. Int. Ed. Engl. (2020) https://doi.org/, doi:10.1002/anie.202004603.

[29] M. Seralathan, S.K. Rangarajan, Scheme of squares: part I. systems formal-ism for potentiostatic studies, J. Electroanal. Chem. Interfacial Electrochem. 191 (1985) 209–228 https://doi.org/, doi:10.1016/S0022-0728(85)80018-8.

[30] J.J. Warren, T.A. Tronic, J.M. Mayer, Thermochemistry of proton-coupled elec-tron transfer reagents and its implications, Chem. Rev. 110 (2010) 6961–7001 https://doi.orghttps://doi.org/, doi:10.1021/cr100085k.

[31] A. Oregioni, B. Stieglitz, G. Kelly, K. Rittinger, T. Frenkiel, Determination of the pKa of the N-terminal amino group of ubiquitin by NMR, Sci. Rep. 7 (2017) 43748 https://doi.org/, doi:10.1038/srep43748.

[32] C. Sissi, L. Lucatello, A. Paul Krapcho, D.J. Maloney, M.B. Boxer, M.V. Camarasa, G. Pezzoni, E. Menta, M. Palumbo, tetra- and heptacyclic perylene analogues as new potential antineoplastic agents based on DNA telomerase inhibition, Biorg. Med. Chem. 15 (2007) 555–562 https://doi.org/, doi:10.1016/j.bmc.2006.09.029.

[33] J.M. Bjuggren, A. Sharma, D. Gedefaw, S. Elmas, C. Pan, B. Kirk, X. Zhao, G. An-dersson, M.R. Andersson, Facile synthesis of an efficient and robust cathode interface material for polymer solar cells, ACS Appl. Energy Mater. 1 (2018) 7130–7139 https://doi.org/, doi:10.1021/acsaem.8b01554.

[34] M. Busch, K. Laasonen, E. Ahlberg, Method for the accurate prediction of elec-tron transfer potentials using an effective absolute potential, PCCP 22 (2020) 25833–25840, doi:10.1039/D0CP04508J.

[35] D.R. Lide, CRC Handbook of Chemistry and Physics: a Ready Reference Book of Chemical and Physical Data, 87, CRC Press, Boca Raton, Florida, 2006 2006-2007.

[36] Z. Luz, S. Meiboom, The activation energies of proton transfer reactions in water, J. Am. Chem. Soc. 86 (1964) 4768–4769 https://doi.org/, doi:10.1021/ja01076a008.

[37] A. Viehbeck, Electrochemical properties of polyimides and related imide com-pounds, J. Electrochem. Soc. 137 (1990) https://doi.org/, doi:10.1149/1.2086690.

[38] C. Hansch, A. Leo, R.W. Taft, A survey of Hammett substituent constants and resonance and field parameters, Chem. Rev. 91 (1991) 165–195 https://doi.org/, doi:10.1021/cr00002a004.

[39] L. Wei, T.S. Zhao, Q. Xu, X.L. Zhou, Z.H. Zhang, In-situ investigation of hydrogen evolution behavior in vanadium redox flow batteries, Appl. Energy 190 (2017) 1112–1118 https://doi.org/, doi:10.1016/j.apenergy.2017.01.039.

[40] C.-.N. Sun, F.M. Delnick, L. Baggetto, G.M. Veith, T.A. Zawodzinski, Hydrogen evolution at the negative electrode of the all-vanadium redox flow batteries, J. Power Sources 248 (2014) 560–564 https://doi.org/, doi:10.1016/j.jpowsour.2013.09.125.